Lithium-Ion Batteries

DOI: 10.1002/ange.200602071

One-Step, Confined Growth of Bimetallic Tin–Antimony Nanorods in Carbon Nanotubes Grown In Situ for Reversible Li^+ Ion Storage

*Yong Wang and Jim Yang Lee**

The discovery of carbon nanotubes (CNTs)[1] has stimulated considerable interest in the synthesis and characterization of one-dimensional nanomaterials. A significant number of materials can now be produced in the form of nanorods or nanowires with diameters ranging from a few to several hundreds of nanometers.[2] One-dimensional electrochemically active materials, such as CNTs,[3,4] CNT-supported SnSb/Sn/SnO_2 particles,[5–8] SnO_2 nanowires, nanorods[9–11] and nanotubes,[12] and SnO_2–CNT duplex nanotubes[13] have been used as the anode of lithium-ion batteries and have delivered significant improvements in application performance over their bulk form. The enhancement effect of the one-dimensional topography should also be applicable to anode materials of a higher caliber. Intermetallic Sn–Sb compounds, which are known for their high specific capacities (relative to graphite) and good cyclability (relative to Sn) because of the reversibility in implementing the lithium insertion and extraction reactions in a stepwise manner,[14–21] spring to mind.

However, the synthesis of Sn–Sb nanorods has yet to be reported. Although Sn–Sb nanoparticles are usually prepared by the reductive co-precipitation of Sn and Sb with $NaBH_4$[14–16,19–21] or Zn,[17,18] the extreme reaction conditions are not conducive to the control of product morphology. The low melting points of Sn and SnSb alloys (ca. 230–240 °C) and the difficulty in composition control have also ruled out the use of a number of popular methods such as thermal evaporation and electrochemical co-deposition of the constituent metals into the pores of hard templates. Herein, we report that bimetallic Sn–Sb nanorods are produced in CNT templates formed in situ. The CNT-encapsulated Sn–Sb nanorods thus obtained show high specific capacities and good cyclability when tested as the anode of lithium-ion batteries.

The field-emission scanning electron microscopy (FESEM) and transmission electron microscopy (TEM) images of the commercial antimony tin oxide (ATO) nanoparticles that were used as the precursor for Sn–Sb nanorod growth can be found in Figure S1 of the Supporting Information. The products obtained from the decomposition of C_2H_2 over ATO are shown in Figure 1a, a large number of rod-like structures approximately 800 nm to 3.5 μm in length and with a uniform diameter are found. Under high magnification (see FESEM image in Figure 1b) the nanorods show a coaxially integrated core–shell structure that consists of a Sn–Sb core and a CNT shell, with no void space between the two. The tips of a few CNTs that have not been completely filled with Sn–Sb. The expanded view of a partially filled CNT tip and that of a completely filled CNT tip are shown in Figure 1c and Figure 1d, respectively. Powder X-ray diffraction (XRD)

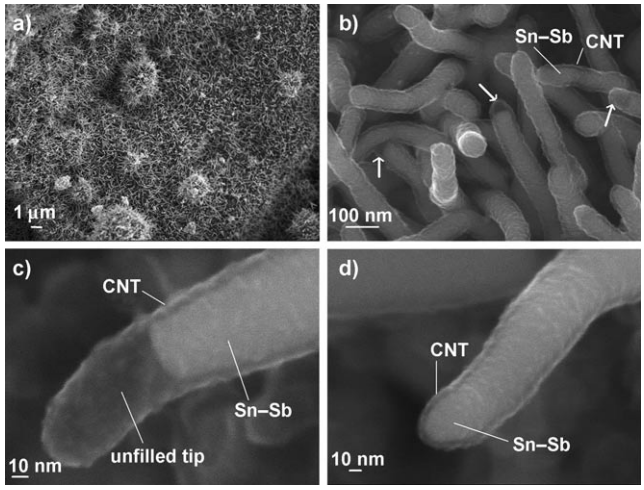

Figure 1. FESEM images of the CNT-encapsulated Sn–Sb nanorods showing a) a large number of rod-like products at low magnification, b) the thin CNT overlayer of filled nanorods at high magnification, the tips of a few CNTs that have not been completely filled with Sn–Sb are indicated by arrows, c) the unfilled tip of a filled CNT, and d) the completely filled tip of a filled CNT.

[*] Dr. Y. Wang, Prof. Dr. J. Y. Lee
Department of Chemical and Biomolecular Engineering
National University of Singapore
10 Kent Ridge Crescent, 119260 Singapore (Singapore)
Fax: (+65) 6779-1936
E-mail: cheleejy@nus.edu.sg
Homepage: http://www.chee.nus.edu.sg/staff/lee.html

Supporting Information for this article is available on the WWW under http://www.angewandte.org or from the author.

measurements (see Figure S2 in the Supporting Information) confirmed that the filling is a multiphase mixture of Sn and SnSb. inductively coupled plasma (ICP) spectroscopy and CHN elemental analysis of the core–shell nanorods gave the following composition: approximately 7.6 wt% of CNTs and approximately 92.4 wt% of Sn–Sb, with an overall stoichiometry of $SnSb_{0.11}$.

The TEM images in Figure 2a and Figure 2b show the tips of two free-standing CNTs one with and one without complete filling of their cores by Sn–Sb. The carbon shell is about 7–10 nm thick and the diameter of the Sn–Sb core is

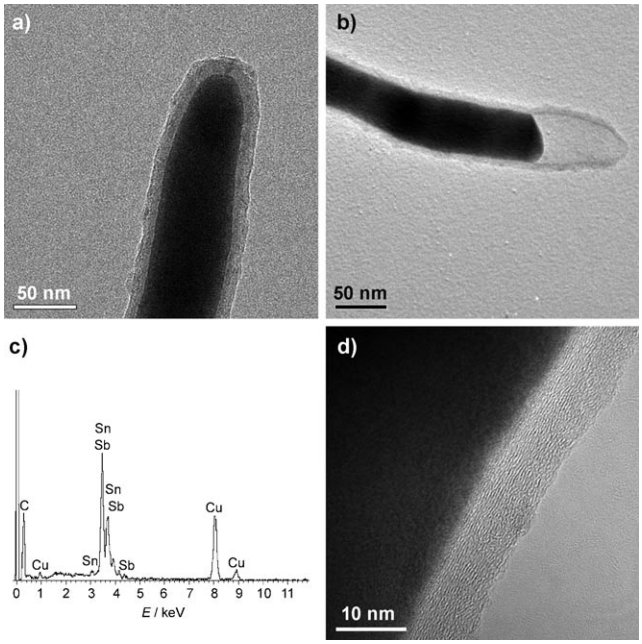

Figure 2. TEM images of a CNT-encapsulated Sn–Sb nanorod: a) a completely filled CNT tip, b) expanded view of a partially filled tip, c) EDS analysis of a CNT-encapsulated Sn–Sb nanorod, d) HRTEM image of a CNT encapsulated Sn–Sb nanorod showing the multiwalled structure of the CNT sheath.

about 70 nm. Energy-dispersive X-ray spectroscopy (EDS) of the core–shell structure in Figure 2c confirmed the presence of Sn and Sb. The measured Sn/Sb atomic ratio of about 8:1 is in good agreement with the ratio in the ATO nanoparticles and suggests no selective incorporation of either of the metals into the CNT interior. During the TEM examination of the core–shell structure (see Figure S3 in the Supporting Information) a number of Sn–Sb nanorods melted after a few minutes of electron-beam irradiation. This phenomenon, which is common for low-melting metals, such as Sn (232 °C),[22] In (157 °C),[23] and Bi (271 °C),[24] is the result of localized heating by the focused electron beam. The high resolution (HR)TEM image in Figure 2d shows that the carbon shell is made up of staggered, shortened graphene sheets. This less graphitic form of carbon could promote Li^+ ion diffusion into the Sn–Sb core through the "gaps" in the graphene sheets so that Li^+ ions need not enter only through the ends of the CNTs. There is some low level residual hydrogen in the CNTs (H/C weight ratio = 0.39%), although this should have only a minor effect on lithium-ion storage.[25]

Based on the experimental observations, a growth mechanism for the CNT-encapsulated Sn–Sb nanorods may be proposed: ATO is first reduced by C_2H_2 to form low-melting (ca. 230–240 °C) Sn–Sb intermetallic compounds which catalyze the growth of CNTs by C_2H_2 decomposition. Since no residual catalyst particles are found at the CNT tips (the closed end of the nanotube, see Figure 1b,c and 2b), the growth of CNTs is believed to occur by the "bottom-up" mechanism. At the high growth-temperature of 700 °C, the low-melting Sn–Sb intermetallic compounds are present as liquid droplets from which the CNTs grow. Capillary forces then draw the liquid droplets into the interior of the CNTs once the latter have grown to a sufficient length. In this way the CNTs formed in situ are the hard template[26,27] that shapes the molten Sn–Sb into nanorods (upon cooling) and prevents the coalescence of molten Sn–Sb into large spherical droplets. Figure 3 shows a schematic sketch of the perceived

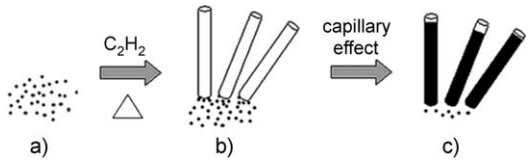

Figure 3. Schematic representation of the in situ growth of Sn–Sb nanorods inside carbon nanotubes. a) Antimony tin oxide nanoparticles. b) Growth of carbon nanotubes induced by molten Sn–Sb alloy. c) Capillary encapsulation of molten Sn–Sb into carbon nanotube interior.

growth process. It should be emphasized that the CNT shell is formed by the catalytic action of Sn–Sb rather than by the physical deposition of carbon onto fully developed Sn–Sb nanorods. This situation is evident from the presence of a considerable number of CNTs with unfilled Sn–Sb sections near their closed ends (Figure 1b). In addition, the low-melting Sn–Sb cannot be in the solid state at the high temperature of this process, let alone in a rod-like morphology that is energetically much less favorable than a spherical geometry.

The capillary encapsulation technique has been used previously to induct filler materials into prefabricated CNTs.[5,28,29] It requires the CNTs to be opened by chemical means. However, the filler material is often found on the CNT exterior because of the small pore and large aspect ratio of the CNTs, and most preparations require the "immersion" of CNTs in the filler material. The yield for the filling process is therefore often low.[5,29] The method presented herein, however, delivers a very high filling yield using CNTs that are grown in situ from an initial pool of the filler (Sn–Sb) material. Besides being the catalyst for the CNT growth, the liquid Sn–Sb droplets are also the source for sustaining the uninterrupted encapsulation of Sn–Sb through the collaborative action of the wicking effect (to draw in the molten liquid) and continuing CNT growth. This in situ process is highly efficient, as shown by the experimental findings that the process consumes most of the supplied Sn–Sb material,

with practically no Sn–Sb remaining on the CNT exterior walls.

Sn–Sb was first identified as a promising anode material for lithium-ion batteries by the Besenhard group.[14] Lithium ions first insert into a more active (relative to Sn) Sn–Sb phase at around 0.7–0.8 V (vs. Li^+/Li), forming Li_3Sb and Sn phases in the process. Then Li ions insert into the Sn phase at 0.66 V or lower.[14–21] The inactive components (Sn during Li^+ insertion into Sn–Sb and Li_3Sb during Li^+ insertion into Sn) are used as the matrix to "buffer" the volume expansion in the alloying reaction, thereby improving the mechanical stability and consequently cyclability of the anode compared to a single Sn phase.[14–21] The above-mentioned stepwise insertion could be identified by the voltage plateaus in the first two cycles of the charge and discharge curves (see Figure S4 in the Supporting Information).

Figure 4 shows the cycling performance of a CNT-encapsulated Sn–Sb nanorod anode. Except for the first cycle, where coulombic efficiencies are 74.4% and 64.3% for the 5 mV–2 V and 0.1 V–1.2 V windows, respectively, the rest

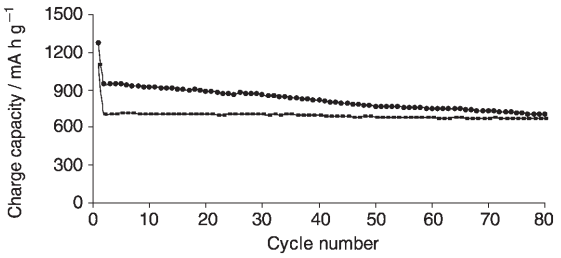

Figure 4. Cyclability of CNT-encapsulated Sn–Sb nanorods in the 5 mV–2 V (●, upper trace) and 0.1 V–1.2 V (vs. Li^+/Li) voltage windows (■, lower trace). Charge and discharge rate: ca. 0.2 C.

of the cycles are about 100% coulombic efficient. The CNT-encapsulated Sn–Sb nanorods are able to sustain high specific capacity in the neighborhood of 900 mA h g^{-1} for at least 30 cycles in the 5 mV–2 V range. This remarkably high capacity can be attributed to the rod-like morphology of Sn–Sb. It has been suggested that storage capacity is higher in one-dimensional nanomaterials because lithium-ion diffusion is facilitated.[30–32] Lithium ions could also be stored in the space between stacks of collapsed nanorods[30] and in the CNT shell. While the material still experiences discernible capacity fading after 80 cycles, this performance is nevertheless a significant improvement over previous efforts (a capacity reduction from 948 to 861 mA h g^{-1} in 30 cycles compared to a capacity reduction from 800 to about 200 mA h g^{-1} in 30 cycles[20]). The rate of capacity fading (ca. 0.3% loss per cycle) is substantially slower than those of SnO_2 nanowires[11] (ca. 3.9% loss per cycle) and SnO_2 nanorods[10] (ca. 1.2% loss per cycle). When tested in the narrower voltage window of 0.1–1.2 V,[16,19] the CNT-encapsulated Sn–Sb nanorods show an even more stable cycling performance. The specific capacity was found to be 672 mA h g^{-1} after 80 cycles, which corresponds to 94.9% retention of the initial capacity (708 mA h g^{-1}). The average fade rate of only 0.064% per cycle is excellent for this class of materials and has not been witnessed for Sn–Sb based anodes to date. The specific capacity (ca. 700 mA h g^{-1}) is lower in the 0.1–1.2 V voltage window, as expected, but it still greatly exceeds what is possible with Sn–Sb particles (500–600 mA h g^{-1}, 0.1–1.2 V).[16,19] Although the CNT shell only amounts to 7.6% of the composite weight, this thin skin of carbon is robust enough to keep the Sn–Sb in good electrical and mechanical contact. This feature has long been recognized as the key factor for prolonging the cyclability of alloy-based anodes.[33]

In summary, we report the confined growth of Sn–Sb nanorods with a previously unreported nanostructure—inside carbon nanotubes—starting from bulk antimony tin oxide particles. The CNT-encapsulated Sn–Sb nanorods contain 7.6 wt% of CNTs (ca. 90 nm in diameter and 7–10 nm in wall thickness) and 92.4 wt% of Sn–Sb nanorods (as $SnSb_{0.11}$; ca. 70 nm in diameter). The CNT skin is able to hinder the coalescence of molten Sn–Sb droplets at high temperatures and it also improves the electrical connectivity and mechanical integrity of the Sn–Sb nanorods. These CNT-encapsulated Sn–Sb nanorods, when tested as the anode material for lithium-ion batteries, display very high specific capacities and good cycling performance for this class of material. This method of fabrication should also be explored for other low-melting Li-alloying metals, such as Sn–Cu,[34] Sn–Fe,[35] and Sn–Ni.[36]

Experimental Section

Preparation of CNT-encapsulated Sn–Sb nanorods: Commercial antimony tin oxide nanoparticles (Aldrich, ATO, $Sb_3O_4{\cdot}SnO_2$, mean particle size: 19 nm; Sb_3O_4: 7–11 wt%; SnO_2: 89–93 wt%; 0.2 g) were uniformly distributed on an aluminum foil in a crucible. The crucible was heated in a tubular furnace under flowing C_2H_2 (10% C_2H_2 and 90% N_2; 200 sccm) at 700 °C for 4 h before the furnace was cooled naturally in the same gas mixture to room temperature. The recovered product was obtained as a black powder.

Characterization: The CNT-encapsulated Sn–Sb nanorods were characterized by FESEM (JEOL JSM-6700F), TEM and EDS (JEOL JEM-2010F), HRTEM (Philips FEG-CM300), and powder XRD (Shimadzu XRD-6000, $Cu_{K\alpha}$ radiation).

Electrochemical measurements: The working electrode was formulated from a mixture of 80 wt% of CNT-encapsulated Sn–Sb nanorods, 10 wt% of conductivity agent (carbon black, Super-P), and 10 wt% of binder (polyvinylidene difluoride (PVDF), Aldrich). Lithium foil was used as the counter electrode, and the electrolyte was 1M $LiPF_6$ in a 50:50 (w/w) mixture of ethylene carbonate (EC) and diethyl carbonate (DEC). More details on the electrode fabrication and cell assembly can be found elsewhere.[10,12] All cells were tested galvanostatically at a rate of about 0.2 C (ca. 0.2 mA cm^{-2} or 180 mA g^{-1}) and were charged (Li^+ insertion) and discharged (Li^+ extraction) between fixed voltage limits (5 mV–2 V or 0.1 V–1.2 V).

Received: May 24, 2006
Revised: August 23, 2006
Published online: September 29, 2006

Keywords: alloys · antimony · electrochemistry · lithium · tin

[1] S. Iijima, *Nature* **1991**, *354*, 56.
[2] C. N. R. Rao, F. L. Deepak, G. Gundiah, A. Govindaraj, *Prog. Solid State Chem.* **2003**, *31*, 5.

[3] G. Che, B. B. Lakshmi, E. R. Fisher, C. R. Martin, *Nature* **1998**, *393*, 346.
[4] H. Shimoda, B. Gao, X. P. Tang, A. Kleinhammes, L. Fleming, Y. Wu, O. Zhou, *Phys. Rev. Lett.* **2002**, *88*, 015502.
[5] T. P. Kumar, R. Ramesh, Y. Y. Lin, G. T. K. Fey, *Electrochem. Commun.* **2004**, *6*, 520.
[6] W. X. Chen, J. Y. Lee, Z. L. Liu, *Electrochem. Commun.* **2002**, *4*, 260.
[7] Z. P. Guo, Z. W. Zhao, H. K. Liu, S. X. Dou, *Carbon* **2005**, *43*, 1392.
[8] J. Xie, V. K. Varadan, *Mater. Chem. Phys.* **2005**, *91*, 274.
[9] N. Li, C. R. Martin, *J. Electrochem. Soc.* **2001**, *148*, A164.
[10] Y. Wang, J. Y. Lee, *J. Phys. Chem. B* **2004**, *108*, 17832.
[11] Z. Ying, Q. Wan, H. Cao, Z. T. Song, S. L. Feng, *Appl. Phys. Lett.* **2005**, *87*, 113108.
[12] Y. Wang, J. Y. Lee, H. C. Zeng, *Chem. Mater.* **2005**, *17*, 3899.
[13] Y. Wang, H. C. Zeng, J. Y. Lee, *Adv. Mater.* **2006**, *18*, 645.
[14] J. Yang, M. Winter, J. O. Besenhard, *Solid State Ionics* **1996**, *90*, 281.
[15] J. Yang, M. Wachtler, M. Winter, J. O. Besenhard, *Electrochem. Solid-State Lett.* **1999**, *2*, 161.
[16] J. Yang, Y. Takeda, N. Imanishi, O. Yamamoto, *J. Electrochem. Soc.* **1999**, *146*, 4009.
[17] H. Li, G. Zhu, X. Huang, L. Chen, *J. Mater. Chem.* **2000**, *10*, 693.
[18] H. Li, L. Shi, W. Lu, X. Huang, L. Chen, *J. Electrochem. Soc.* **2001**, *148*, A915.
[19] M. Wachtler, J. O. Besenhard, M. Winter, *J. Power Sources* **2001**, *94*, 189.
[20] H. Mukaibo, T. Osaka, P. Reale, S. Panero, B. Scrosati, M. Wachtler, *J. Power Sources* **2004**, *132*, 225.
[21] S. A. Needham, G. X. Wang, H. K. Liu, *J. Alloys Compd.* **2005**, *400*, 234.
[22] J. Hu, Y. Bando, J. Zhan, D. Golberg, *Angew. Chem.* **2004**, *116*, 4706; *Angew. Chem. Int. Ed.* **2004**, *43*, 4606.
[23] Y. Li, Y. Bando, D. Golberg, *Adv. Mater.* **2003**, *15*, 581.
[24] Y. Li, J. Wang, Z. Deng, Y. Wu, X. Sun, D. Yu, P. Yang, *J. Am. Chem. Soc.* **2001**, *123*, 9904.
[25] T. Zheng, J. S. Xue, J. R. Dahn, *Chem. Mater.* **1996**, *8*, 389.
[26] X. R. Ye, Y. Lin, C. Wang, C. M. Wai, *Adv. Mater.* **2003**, *15*, 316.
[27] L. W. Yin, Y. Bando, Y. C. Zhu, M. S. Li, C. C. Tang, D. Golberg, *Adv. Mater.* **2005**, *17*, 213.
[28] P. M. Ajavan, S. Iijima, *Nature* **1993**, *361*, 333.
[29] L. Zhao, L. Gao, *Carbon* **2004**, *42*, 3251.
[30] R. Dominko, D. Arcon, A. Mrzel, A. Zorko, P. Cevc, P. Venturini, M. Gaberscek, M. Remskar, D. Mihailovic, *Adv. Mater.* **2002**, *14*, 1531.
[31] J. Chen, Z. L. Tao, S. L. Li, *Angew. Chem.* **2003**, *115*, 2197; *Angew. Chem. Int. Ed.* **2003**, *42*, 2147.
[32] J. Chen, L. Xu, W. Li, X. Gou, *Adv. Mater.* **2005**, *17*, 582.
[33] M. Winter, J. O. Besenhard, *Electrochim. Acta* **1999**, *45*, 31.
[34] H. C. Shin, M. Liu, *Adv. Funct. Mater.* **2005**, *15*, 582.
[35] O. Mao, J. R. Dahn, *J. Electrochem. Soc.* **1999**, *146*, 414.
[36] G. M. Ehrlich, C. Durand, X. Chen, T. A. Hugener, F. Spiess, S. L. Suib, *J. Electrochem. Soc.* **2000**, *147*, 886.

